JOURNAL OF GUIDANCE, CONTROL, AND DYNAMICS
Vol. 16, No. 1, January–February 1993

Fixed-Order Dynamic Compensation for a High-Performance Fighter Aircraft

Edward V. Byrns Jr.*
Systems Planning and Analysis, Inc., Falls Church, Virginia 22041
and
Anthony J. Calise†
Georgia Institute of Technology, Atlanta, Georgia 30332

This paper presents a robust fixed-order dynamic compensator design for a high-performance fighter aircraft. The compensator design methodology is based on an approximate loop transfer recovery technique. Full-state gains are first designed for the dual system, which is the equivalent of designing a full-order observer. Then the loop characteristics at the dual system input are approximated with a compensator in controller canonical form. Finally, the optimal gains are implemented in the dual compensator to insure robustness and tracking performance at the plant output. The fixed-order dynamic compensator developed here is compared with a previously published full-order observer design.

Introduction

THE agility of modern fighter aircraft is rapidly improving. New flight regimes are being encountered where conventional aerodynamic controls lose their effectiveness. To overcome this difficulty, many new control surfaces are being introduced into the airframe. The coordination of these multiple surfaces is a challenging modern control problem. Classical design techniques are typically difficult to implement.

A version of the Navy's F-18 fighter aircraft has been configured for low-speed, high angle-of-attack flight. Numerous independent inputs are available to control the aircraft. As listed in Ref. 1, these control elements are 1) a large span, single-slotted trailing-edge flap capable of 45-deg deflection in the landing configuration, but doubling as a differential flaperon with ±8-deg deflection in the up and away maneuvering configuration; 2) single-slotted, drooped ailerons for takeoff and landing, with ±25-deg deflection for up and away conditions; 3) leading-edge flaps that are scheduled with angle of attack and Mach number to a maximum of 34 deg down (in addition, they are used differentially ±3 deg for roll augmentation); 4) twin rudders that are used for the normal purposes of directional control and roll coordination but that are also used for enhancement of longitudinal stability and control in the takeoff and landing configurations; 5) an all-movable stabilator with differential deflection for roll; 6) a throttle position that regulates the thrust delivered by the engine; and 7) a thrust vectoring vane system that regulates the angle at which the thrust is applied on the aircraft. This vehicle, the F-18/HARV (High Alpha Research Vehicle), is called "supermaneuverable" since it has thrust vectoring vanes that allow moment generation even in low-speed flight.

In Refs. 1 and 2, several longitudinal flight controllers were designed for the F-18/HARV. Both standard loop transfer recovery (LTR)[3] and H_∞[4] design techniques are employed. These designs produced full-order controllers that provided robustness to unstructured uncertainty at the plant output. In this paper, a fixed-order dynamic compensator is designed for the F-18/HARV, and it is compared with the full-order observer in Refs. 1 and 2. The H_∞ full-order controller is compared with a fixed-order dynamic compensator in Ref. 5.

Fixed-order dynamic compensators are a promising approach to designing low-order controllers. The compensator order is selected at the outset of the design, and this constraint is included in the derivation of the necessary conditions for optimality. However, until recently, the compensator designs had poor robustness characteristics. In Ref. 6, a design technique is presented for approximating recovering linear quadratic regulator (LQR) properties at the plant input when implementing a fixed-order dynamic compensator in either observer or controller canonical form.[7] This formulation parallels the well-known LTR design technique.[3] Full-state gains are first computed for desirable loop properties at the plant input, followed by the compensator design to approximately recover these characteristics. It has also been shown in Ref. 8 that the approximate LTR formulation at the plant output is the exact dual of the procedure in Ref. 6. In this paper, the output approximate LTR technique is used to insure robustness and tracking at the plant output.

A brief outline of this paper follows. First, the observer and controller canonical compensator forms are presented, followed by a review of the approximate LTR design methodologies. Next, the compensator design and implementation steps are discussed. Finally, the detailed design of an F-18/HARV longitudinal flight controller is presented. In this example, the fixed-order dynamic compensator is compared with a full-order observer designed using the standard LTR procedure.

Canonical Compensators

In Ref. 7, a formulation based on observer and controller canonical structures was first presented for designing fixed-order dynamic compensators. The order of the compensator is first selected, and then its structure determined by the choice of either controllability or observability indices. These canonical forms are reviewed later, including a mild extension to the case of proper plants.

Consider the standard linear multivariable system, where x is an n-dimensional vector, u is an m-dimensional vector, and y is a p-dimensional vector.

$$\dot{z} = Ax + Bu \tag{1}$$

$$y = Cx + Du \tag{2}$$

which has the transfer function from u to y

$$G(s) = C\Phi B + D, \qquad \Phi = (sI - A)^{-1} \tag{3}$$

Received July 3, 1991; revision received May 18, 1992; accepted for publication May 29, 1992.

*Analyst; formerly Graduate Research Assistant, School of Aerospace Engineering, Georgia Institute of Technology. Member AIAA.

†Professor, School of Aerospace Engineering. Associate Fellow AIAA.

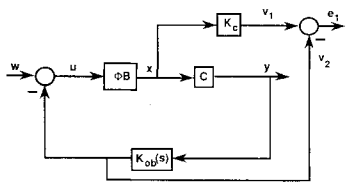

Fig. 1 Approximate LTR formulation for recovery at the plant input.

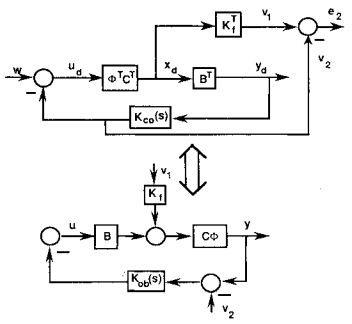

Fig. 2 Approximate LTR formulation for recovery at the plant output.

A compensator in observer canonical form for the system in Eqs. (1) and (2) is given next, where z and u_o are nc-dimensional vectors:

$$\dot{z} = P_{\text{ob}}^o z + u_o \tag{4}$$

$$u_o = P_{\text{ob}} u - Ny \tag{5}$$

$$u_o = -H^o z \tag{6}$$

where P_{ob} and N are free parameter matrices of compatible dimensions. The matrices P_{ob}^o and H^o are predetermined by the choice of observability indices ν_i and their structure is given next:

$$P_{\text{ob}}^o = \text{Block diag}[P_1^o, \ldots, P_m^o] \tag{7}$$

$$P_i^o = \begin{bmatrix} 0 & 0 & 0 & 0 \\ 1 & 0 & \cdots & 0 \\ 0 & 1 & 0 & 0 \\ & & \vdots & \\ 0 & 0 & \cdots & 0 \\ 0 & 0 & 1 & 0 \end{bmatrix}_{\nu_i \times \nu_i} \tag{8}$$

$$H^o = \text{Block diag}\{[0, \ldots, 0 \;\; 1]_{1 \times \nu_i}, i = 1, \ldots, m\} \tag{9}$$

The observability indices are subject to the following constraints:

$$\sum_{i=1}^{m} \nu_i = nc \tag{10}$$

$$\nu_i \leq \nu_i + 1 \tag{11}$$

The open-loop transfer function $K_{\text{ob}}(s)$ from y to u is

$$K_{\text{ob}}(s) = H^o(sI - \boldsymbol{P}_{\text{ob}})^{-1} N \tag{12}$$

where

$$\boldsymbol{P}_{\text{ob}} = P_{\text{ob}}^o - P_{\text{ob}} H^o \tag{13}$$

A controller canonical compensator for the system in Eqs. (1) and (2) is formulated in Eqs. (14–16), where z_c is an nc-dimensional vector, and u_c is a p-dimensional vector:

$$\dot{z}_c = P_c^o z_c + N^o u_c - N^o y \tag{14}$$

$$u_c = -P_c z_c \tag{15}$$

$$u = -Hz_c \tag{16}$$

where P_c and H are the free parameter matrices. In this case, the matrices P_c^o and N^o are predetermined by the choice of controllability indices, ν_i, and their structure is given next:

$$P_c^o = \text{Block diag}[P_1^o, \ldots, P_p^o] \tag{17}$$

$$P_1^o = \begin{bmatrix} 0 & 1 & 0 & \cdots & 0 & 0 \\ 0 & 0 & 1 & \cdots & 0 & 0 \\ & & & \vdots & & \\ 0 & 0 & 0 & \cdots & 0 & 1 \\ 0 & 0 & 0 & \cdots & 0 & 0 \end{bmatrix}_{\nu_i \times \nu_i} \tag{18}$$

$$N^o = \text{Block diag}\{[0, \ldots, 0 \;\; 1]_{\nu_i \times 1}^T, i = 1, \ldots, p\} \tag{19}$$

The controllability indices are subject to the following constraints:

$$\sum_{i=1}^{p} \nu_i = nc \tag{20}$$

$$\nu_i \leq \nu_i + 1 \tag{21}$$

In this form, the open-loop transfer function $K_{co}(s)$ from y to u is

$$K_{co}(s) = H(sI - \boldsymbol{P}_{co})^{-1} N^o \tag{22}$$

where

$$\boldsymbol{P}_{co} = P_c^o - N^o P_c \tag{23}$$

Note that these compensator structures are also constrained to be strictly proper.

For both of these canonical forms, the design of the free parameter matrices reduces to a constant gain output feedback problem when the plant dynamics are adjoined with the compensator dynamics. Because of the structure of the two canonical compensators, $N^o = H^{oT}$ and $P_c^o = P_{\text{ob}}^{oT}$ for the same set of observability and controllability indices. Therefore, the

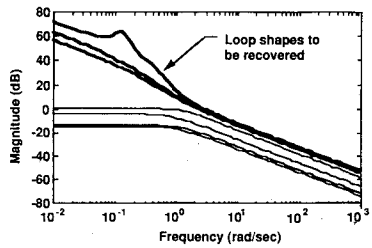

Fig. 3 Loop shapes for the F-18 full-order observer.

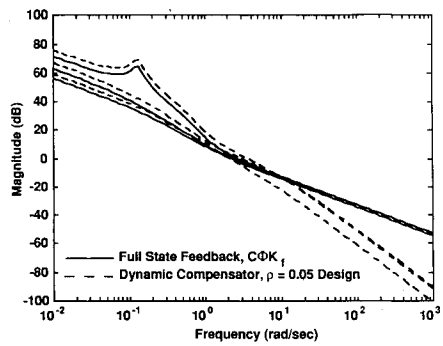

Fig. 4 Loop transfer function with the loop broken at the plant output.

observer canonical compensator of Eqs. (4–6) is the exact dual of the controller canonical form of Eqs. (13–15) (for the same set of compensator indices) if $P_c = P_{ob}^T$ and $H = N^T$.

Approximate LTR Formulations

Recovery at the Plant Input

In Ref. 6, an approximate LTR method is presented for recovery of loop properties at the plant input. This formulation is based on a performance index that penalizes the difference between two closed-loop return signals, corresponding to $\mathbf{v}_1$ and $\mathbf{v}_2$ in Fig. 1. These signals are produced by identical uniformly distributed impulses injected at the plant input for zero initial conditions. It has been shown that if $\mathbf{v}_2 \rightarrow \mathbf{v}_1$, then $K_{ob}G$ approximates $K_c\Phi B$.[8]

If the compensator is defined using the observer form, then the signal error is given by

$$e_1 = \mathbf{v}_1 - \mathbf{v}_2 = K_c x - H^o z \tag{24}$$

where the full-state gain K_c is designed for desirable loop properties at the plant input. In this context, it can be seen from Eq. (24) that the observer form has the unique advantage in that H^o is a predefined matrix. The approximate LTR performance index is

$$J = E_{x_0}\left\{\int_0^\infty [e_1^T e_1 + \rho u_o^T u_o]\, dt\right\} \tag{25}$$

As the parameter $\rho \rightarrow 0$, then $K_{ob}G$ approximates $K_c\Phi B$ to varying degrees depending on the order of the compensator. This problem can be reduced to a standard constant gain output feedback design formulation wherein the plant and compensator state weighting matrices and the resulting distribution on initial conditions (due to the impulsive inputs) are uniquely defined.[6]

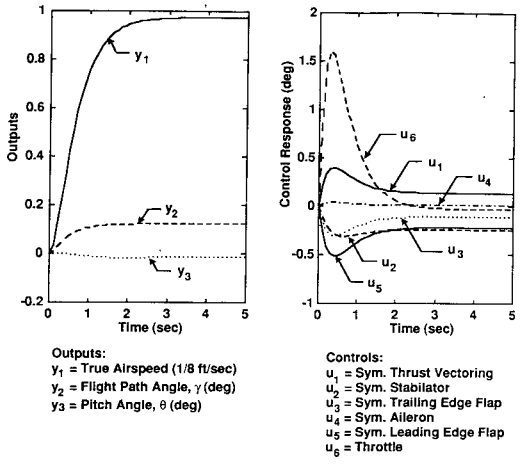

Fig. 5 System response to a step $\mathbf{v}_T$ command.

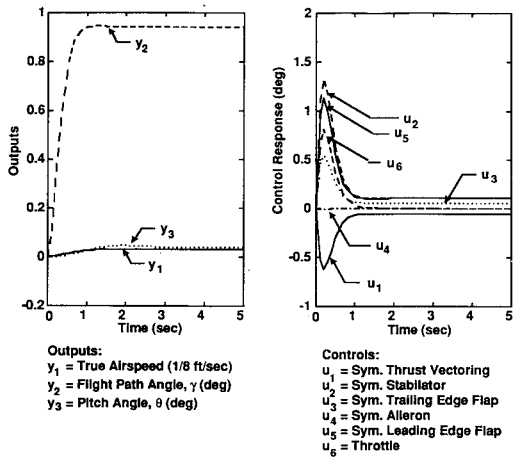

Fig. 6 System response to a step γ command.

Recovery at the Plant Output

An approximate LTR methodology at the plant output is the exact dual of the input recovery problem.[8] To formulate this problem, consider the dual of Eqs. (1) and (2) given next, where x_d is an n-dimensional vector, u_d is a p-dimensional vector, and y_d is an m-dimensional vector:

$$\dot{x}_d = A^T x_d + C^T u_d \tag{26}$$

$$y_d = B^T x_d + D^T u_d \tag{27}$$

A full-state gain matrix K_f^T is computed to produce desirable loop shapes at the dual plant input. This is equivalent to designing full-order observer gains to insure the loop properties at the plant output.[3]

Assuming an observer canonical form is to be implemented, then a compensator in the controller form is first designed to recover the loop properties at the dual plant input. Note that in this case $u_d = -Hz_c$. Referring to Fig. 2, this corresponds to a penalty on the difference between $\mathbf{v}_1$ and $\mathbf{v}_2$, with the result that $K_{co}G^T$ approximates $K_f^T\Phi^T C^T$. The error signal in this case is given by

$$e_2 = \mathbf{v}_1 - \mathbf{v}_2 = K_f^T x_d - Hz_c \tag{28}$$

and the approximate LTR performance index becomes

$$J = E_{x_0}\left\{\int_0^\infty [e_2^T e_2 + \rho u_c^T u_c]\, dt\right\} \tag{29}$$

The reduction to a standard constant gain output feedback design formulation in this case is slightly more complicated in that the error term in Eq. (28) now depends on H, which is a free parameter matrix. Substitution of Eq. (28) into Eq. (29) introduces a cross term between x_d and u_d in the performance index, the details for which are given later. Again, as $\rho \rightarrow 0$, then $K_{co}G^T$ approximates $K_f^T\Phi^T C^T$, and transposing this relationship yields GK_{co}^T approximates $C\Phi K_f$. Because of the structure of the canonical compensators, K_{co}^T designed for the dual sysetm in Eqs. (26) and (27) is equivalent to K_{ob} constructed for the original plant in Eqs. (1) and (2). Therefore, by implementing the observer canonical form, GK_{ob} approximates $C\Phi K_f$, indicating that the dynamic compensator approximately recovers the plant output loop shapes.

Compensator Design and Implementation: Observer Canonical Compensator Implementation

To implement the compensator in observer canonical form, a controller canonical compensator is designed for the dual system. In this case, the reduction to a constant gain output feedback design formulation is slightly more complicated than the approximate LTR methodology of Ref. 6. The details of this formulation are given next.

The dual plant dynamics, Eqs. (26) and (27), are augmented with the controller canonical compensator dynamics, Eqs. (14–16), and the equivalent linear system is given, where $\boldsymbol{x}$ is an $n + nc$ dimensional vector, $\boldsymbol{u}$ is a $p + m$ dimensional vector, and y is an nc-dimensional vector:

$$\dot{\boldsymbol{x}} = \boldsymbol{A}\boldsymbol{x} + \boldsymbol{B}\boldsymbol{u} \tag{30}$$

$$y = \boldsymbol{C}\boldsymbol{x} \tag{31}$$

$$\boldsymbol{u} = -\boldsymbol{G}y \tag{32}$$

where $\boldsymbol{x}^T = \{x_d^T, z_c^T\}$, $\boldsymbol{u}^T = \{u_d^T, u_c^T\}$, $y = z_c$, and

$$\boldsymbol{A} = \begin{bmatrix} A^T & 0 \\ -N^o B^T & P_c^o \end{bmatrix} \qquad \boldsymbol{B} = \begin{bmatrix} C^T & 0 \\ -N^o D^T & N^o \end{bmatrix} \tag{33}$$

$$C = [0 \ I_{nc}] \qquad G = \begin{bmatrix} H \\ P_c \end{bmatrix} \tag{34}$$

As noted earlier, the error signal to be penalized is given by

$$e_2 = \mathbf{v}_1 - \mathbf{v}_2 = K_f^T x_d - Hz_c \tag{35}$$

where $u_d = -Hz_c$, and the approximate LTR performance index becomes

$$J = E_{x_0}\left\{\int_0^\infty [e_2^T W e_2 + \rho u_c^T u_c]\, dt\right\} \tag{36}$$

The weighting matrix, $W \geq 0$, allows the individual error signals to be selectively penalized in the approximate recovery design process. Substituting Eq. (35) into Eq. (36) and rewriting the performance index as

$$J = E_{x_0}\left\{\int_0^\infty [x^T Q x + 2u^T S x + u^T R u]\, dt\right\} \tag{37}$$

yields the following plant and compensator state weighting matrices:

$$Q = \begin{bmatrix} K_f W K_f^T & 0 \\ 0 & 0 \end{bmatrix} \qquad S = \begin{bmatrix} W K_f^T & 0 \\ 0 & 0 \end{bmatrix} \tag{38}$$

$$R = \begin{bmatrix} W & 0 \\ 0 & \rho I_m \end{bmatrix} \tag{39}$$

By injecting uniformly distributed impulses at the dual plant input, the following initial condition variance is produced:

$$E\{x_0 x_0^T\} = X_0 = \begin{bmatrix} C^T C & 0 \\ 0 & 0 \end{bmatrix} \tag{40}$$

Equations (30–32) and (37) constitute a constant gain output feedback problem whose necessary conditions for optimality are well known. Using the basic approach outlined in Ref. 9, the necessary conditions for the output feedback problem defined by Eqs. (30–32) and (37) are derived next. The performance index in Eq. (37) satisfies

$$J = tr\{KX_0\} \tag{41}$$

where K is the solution to

$$A_c^T K + K A_c + AQ + C^T G^T R G C - (C^T G^T S + S^T G C) = 0 \tag{42}$$

$$A_c = A - BGC \tag{43}$$

Defining the Lagrangian as

$$\mathcal{L} = tr\{KX_0 + [A_c^T K + K A_c + Q + C^T G^T R G C - (C^T G^T S + S^T G C)] L^T\} \tag{44}$$

then the necessary conditions for optimality, $\partial\mathcal{L}/\partial K = \partial\mathcal{L}/\partial L = \partial\mathcal{L}/\partial G = 0$, are

$$A_c L + L A_c^T + X_0 = 0 \tag{45}$$

$$A_c^T K + K A_c + AQ + C^T G^T R G C = 0 \tag{46}$$

$$2RGCLC^T - 2B^T K L C^T - 2SLC^T = 0 \tag{47}$$

Solving Eq. (47) for G yields

$$G = R^{-1}[(B^T K + S)LC^T](CLC^T)^{-1} \tag{48}$$

and thus a convergent sequential algorithm[10] can be used to solve the necessary conditions defined by Eqs. (45), (46), and (48). As the design parameter ρ is reduced, the loop properties $K_f^T \Phi^T C^T$ are approximated by $K_{co}(s)G^T(s)$. This determines H and P_c. Using the relationships $N = H^T$ and $P_{ob} = P_c^T$, the optimal gains are implemented in the observer canonical compensator, Eqs. (4–6).

F-18/HARV Longitudinal Flight Controller

This example considers the design of a longitudinal flight controller for the supermaneuverable F-18/HARV. In Refs. 1 and 2, several flight controllers are developed for this vehicle using the standard LTR and H_∞ design techniques. In comparison, this example illustrates the design of a fixed-order dynamic compensator using the output approximate LTR technique. This compensator is then compared with the standard LTR design in Refs. 1 and 2.

F-18/HARV Longitudinal Dynamics

The F-18/HARV four-state linearized longitudinal dynamical model is given in Refs. 1 and 2 for a low-speed, high angle of attack (Mach 0.24, $\alpha = 25$ deg) at 15,000 ft altitude. This flight condition is considered to be a difficult trim point. The state-space representation of the dynamics is given by

$$\dot{x} = \mathfrak{A}x + \mathfrak{B}u \tag{49}$$

where the scaled system matrices are

$$\mathfrak{A} = \begin{bmatrix} -0.0750 & -0.1399 & 0 & -0.1871 \\ -0.1517 & -0.1959 & 0.9896 & 0 \\ -0.0258 & -0.1454 & -0.1877 & 0 \\ 0 & 0 & 1.0 & 0 \end{bmatrix} \tag{50}$$

$$\mathfrak{B} = \begin{bmatrix} -0.3830 & 0 & -0.8258 & 0.0262 & -0.4114 & 1.4400 \\ -0.5157 & -0.3724 & -0.8377 & -0.0054 & -0.5157 & -0.4641 \\ -19.1941 & -2.0054 & -23.3767 & -0.0653 & 1.2032 & 0.7271 \\ 0 & 0 & 0 & 0 & 0 & 0 \end{bmatrix} \tag{51}$$

and the state and control vectors are

$$x = \begin{Bmatrix} \text{true airspeed, } \mathbf{v}_T(1/8 \text{ ft/s}) \\ \text{angle of attack, } \alpha \text{ (deg)} \\ \text{pitch rate (rad/s)} \\ \text{pitch angle (deg)} \end{Bmatrix} \tag{52}$$

$$u = \begin{Bmatrix} \text{symmetric thrust vectoring vane (deg)} \\ \text{symmetric aileron (deg)} \\ \text{symmetric stabilator (deg)} \\ \text{symmetric leading-edge flap (deg)} \\ \text{symmetric trailing-edge flap (deg)} \\ \text{throttle position (deg)} \end{Bmatrix}$$

Note that this model has an unstable phugoid mode at $0.0188 \pm 0.1280j$ and a stable short period mode at $-0.248 \pm 0.3585j$.

Three of the six control inputs are redundant since rank $(\mathcal{B}) = 3$. Following the procedure in Refs. 1 and 2, the actual system, Eq. (49), can be replaced by the pseudosystem

$$\dot{x} = \mathcal{A}x + B_v v \tag{53}$$

where v is a vector of three linearly independent pseudocontrols, and B_v spans the same space as $\mathcal{B}$. Accounting for the structure of $\mathcal{B}$, an appropriate choice for B_v, is

$$B_v = \begin{bmatrix} I_3 \\ 0 \end{bmatrix} \tag{54}$$

A controller can now be designed using the pseudosystem, and as a postdesign step, the pseudocontrols can be mapped onto the actual controls. This transformation is given by

$$u = Tv \tag{55}$$

where

$$T = \mathcal{W}^{-1}B_1^T(B_1\mathcal{W}^{-1}B_1^T)^{-1}, \qquad \mathcal{W} = \text{diag}\{1\ 1\ 1\ 1\ 1.3\ 1\} \tag{56}$$

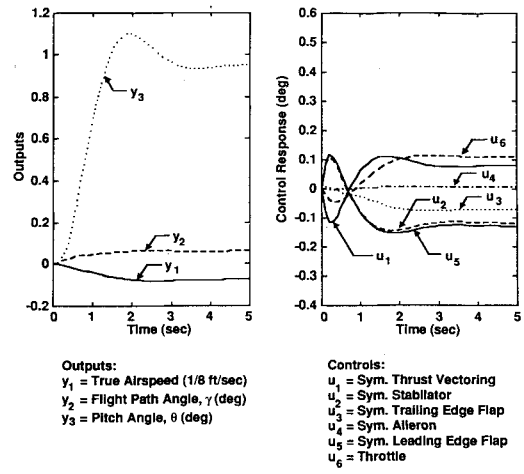

Fig. 7 System response to a step θ command.

and B_1 is the upper 3×6 block of $\mathcal{B}$. This transformation distributes the pseudocontrol so that the weighted energy of the actual redundant control is minimized. This approach also provides for reconfigurable control. The details of this optimization procedure are given in Ref. 2.

To insure type I behavior (zero steady-state error), three integrators are introduced into the system. Defining $x = \{x^T, \int v_T, \int\alpha, \int\theta\}^T$, the augmented system matrices are

$$A = \left[\begin{array}{cccccccc|cc} & & & & & & & & & \\ & & & \mathcal{A} & & & & & + & \\ \hline 1 & 0 & 0 & 0 & 0 & 0 & 0 & | & 0 & 0 \\ 0 & 1 & 0 & 0 & 0 & 0 & 0 & | & 0 & 0 \\ 0 & 0 & 0 & 1 & 0 & 0 & 0 & | & 0 & 0 \end{array}\right] \qquad B = \begin{bmatrix} B_v \\ 0 \\ 0 \\ 0 \end{bmatrix} \tag{57}$$

The outputs of this system are $y = \{v_T, \gamma, \theta, p, \int v_T, \int\alpha, \int\theta\}^T$, where $\gamma = \theta - \alpha$ is the flight-path angle. The v_T, θ, and γ outputs are chosen to maintain compatibility with the previously published designs. The p output is included since pitch rate is normally an available measurement. This measurement set allows for proportional plus integral control.

Dynamic Compensator Design

Using the system matrices in Eq. (57), a full-order observer is first designed by selecting.

$$Q = BB^T \qquad R = 0.2I_7 \tag{58}$$

and the resulting gain matrix is

$$K_f = \begin{bmatrix} 1.3793 & 0.2063 & -0.1082 & -0.0558 & 1.6099 & -0.1329 & -0.0869 \\ -0.1180 & -1.8820 & 0.6326 & 0.5324 & -0.1248 & 0.8904 & 0.3406 \\ -0.0209 & 0.0862 & 0.6186 & 1.9287 & -0.0133 & 0.0717 & 0.0921 \\ -0.0406 & 0.1056 & 0.7382 & 0.6186 & -0.0282 & 0.3145 & 0.4440 \\ 0.6037 & 0.0967 & -0.0282 & -0.0133 & 1.6856 & -0.0545 & -0.0308 \\ -0.0498 & -0.5759 & 0.3145 & 0.0717 & -0.0545 & 1.1176 & 0.3008 \\ -0.0326 & 0.1033 & 0.4440 & 0.0921 & -0.0308 & 0.3008 & 0.7610 \end{bmatrix} \tag{59}$$

In Fig. 3, the singular values of $C\Phi K_f$ are shown. The focus of this design is to recover the first three loop shapes of $C\Phi K_f$, which are associated with the v_T, γ, and θ measurements.

A third-order observer form compensator is to be implemented. Thus, a controller form compensator must first be designed to recover the loop properties at the dual plant input. To maintain compatibility with the standard LTR design in Refs. 1 and 2, only the v_T, γ, and θ loop shapes are to be recovered. Thus, the error signal weighting matrix, W in Eq. (36), is selected as $W = \text{diag}\{1, 1, 1, 1.0E-4, 1.04E-4, 1.04E-4, 1.04E-4\}$. In Fig. 4, the recovery of the desired loop shapes is shown for the $\rho = 0.05$ design. This design is considered to have sufficiently recovered the desired loop shapes. For $\rho = 0.05$, the compensator free parameter matrices are given next:

$$N = \begin{bmatrix} -23.57 & -0.609 & 1.077 & 0.264 & -0.237 & -0.00121 & -0.00131 \\ 2.302 & 30.20 & 1.245 & 0.338 & -0.00285 & -0.252 & 0.123 \\ 0.332 & -0.409 & -22.79 & -14.35 & 0.00111 & -0.104 & -0.206 \end{bmatrix} \tag{60}$$

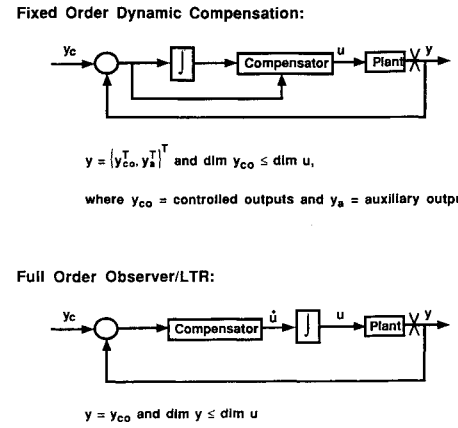

Fig. 8 Comparison of controller structures.

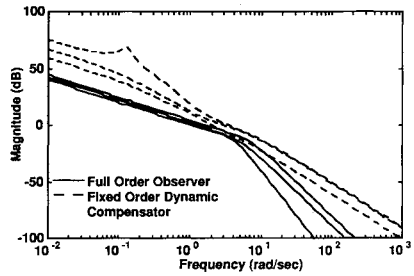

Fig. 9 Comparison of loop transfer functions.

$$P_{ob} = \begin{bmatrix} 6.341 & -0.0909 & -0.0238 \\ -0.0443 & 9.911 & -0.00670 \\ -0.0266 & -0.0184 & 7.093 \end{bmatrix} \tag{61}$$

In Figs. 5–7, time histories are shown for step commands in v_T, γ, and θ, respectively. As a general conclusion, all of the output and control responses appear reasonable. No excessive control deflections are observed in the control channels. The apparent lack of zero steady-state error is actually due to slow integrator modes. Over an extended time interval, this steady-state error disappears. In Fig. 5, the system 90% settling time is less than 3 s, and the maximum control effort is approximately 1.6 deg of throttle. For the γ step command, Fig. 6, the system 90% settling time is around 1 s, and the maximum control effort is approximately 1.3 deg of symmetric stabilator. In this response, the control responses have an extremely quick rise time since the actuator dynamics are not modeled. Finally, the slowest response is the θ channel, where the 90% settling time is near 5 s, Fig. 7. However, in this channel all of the control deflections are extremely small.

Comparison with an Observer Design

In Refs. 1 and 2, a full-order observer is designed for the F-18 using the standard LTR methodology.[3] Unlike the approximate LTR methodology for the fixed-order compensators, the standard LTR design technique requires that the plant be squarable (i.e., number of inputs equals number of outputs). This requirement limits the number of outputs to three, and they are $y = \{v_T, \gamma, \theta\}^T$. In addition, to maintain the square plant, the three integrators must be implemented in series with the control inputs, which is a unconventional configuration. If proportional plus integral control is introduced, as in the fixed-order dynamic compensator design, then the number of outputs would exceed the number of inputs. A block diagram comparison of the standard LTR controller and the fixed-order dynamic compensator is shown in Fig. 8. In this figure, y_{co} corresponds to $\{v_T, \gamma, \theta\}^T$, and y_a corresponds to $\{p, \int v_T, \int \alpha, \int \theta\}^T$.

The loop transfer functions, with the loop broken at the plant output, are compared in Fig. 9 for the full-order observer and the $\rho = 0.05$ compensator design. Both designs have a bandwidth of approximately 3 rad/s. However, the singular values of the full-order observer design are slightly tighter at the crossover frequency. In addition, both controllers provide additional rolloff beginning at approximately 10 rad/s. The increased rolloff for the full-order observer design is due to the greater number of poles in this controller.

In Table 1, the open-loop poles of the full-order observer are compared with the poles of the fixed-order dynamic compensator. Since the fixed-order compensator is not square, there are no transmission zeros for this controller. When the integrator states are included, the full-order observer is a 10-state compensator, whereas the fixed-order dynamic compensator is only a 6-state compensator. However, excluding the three integrator states, the fixed-order compensator has dynamics that are similar to the three fastest full-order observer modes. The fixed-order compensator has a stable pole at 6.34 rad/s, whereas the full-order observer has a stable pole at 5.24 rad/s. The remaining two fixed-order compensator poles are slightly different from the fastest full-order observer mode. The full-order observer has a stable complex pole at $(\omega, \zeta) = (7.46$ rad/s, 0.73), whereas the fixed-order dynamic compensator has two stable real poles at 7.09 and 9.92 rad/s. However, it is interesting to note that in each controller the magnitudes of these two poles do not differ significantly. In fact, the poles of the fixed-order compensator can be characterized by $(\omega, \zeta) = (8.39$ rad/s, 2.03), so the difference is pri-

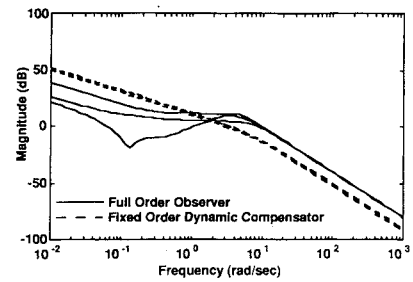

Fig. 10 Singular values of the full-order observer and fixed-order dynamic compensator.

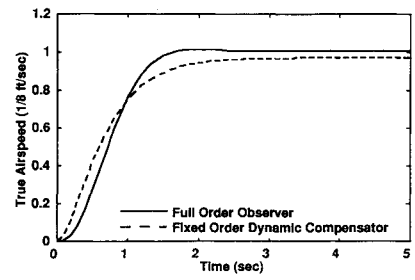

Fig. 11 Comparison of v_T step responses.

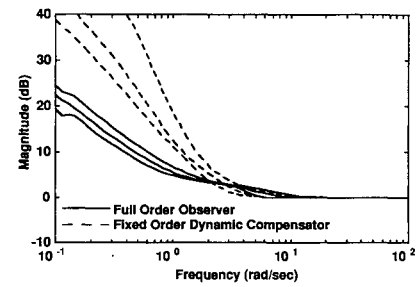

Fig. 12 Comparison of return difference singular values.

Table 1 Comparison of controller characteristics

	Full-order observer	Fixed-order dynamic compensator
No. of inputs	3	7
No. of outputs	3	3
Compensator poles $a \pm bj$	$-5.49 \pm 5.07j$	$-9.92.0$
	-5.24	$-7.09.3$
	$-3.94 \pm 3.32j$	-6.34
	$-2.05 \pm 3.68j$	0, 0, 0
	0, 0, 0	
Compensator zeros $a \pm bj$	$-0.248 \pm 0.359j$	
	$-0.178 \pm 0.124j$	

marily in the damping ratios. In Fig. 10, the singular values of the full-order observer are compared with those of the fixed-order dynamic compensator. Note that both controllers have very similar frequency characteristics.

In Fig. 11, the time response of a step $\mathbf{v}_T$ command is compared for the full-order observer and the fixed-order dynamic compensator. The full-order observer has a response time of approximately 2 s, whereas the fixed-order dynamic compensator has a response time of approximately 4 s. Note that the full-order observer response does not exhibit the slow integrator mode behavior, which is evident in the fixed-order compensator response. However, both trajectories appear reasonable. In Fig. 12, the singular values of the return difference matrix, $[I + G(s)K(s)]$, are compared for the fixed-order dynamic compensator and the full-order observer. For both of these designs, the minimum singular value is 0 dB, which indicates that the designs have recovered all of the robustness properties of the full-state feedback design. Each output channel has a guarantee of 60-deg phase margin and 6 dB gain margin. Thus, it appears that the fixed-order dynamic compensator provides similar robustness and performance properties as the full-order observer, but with the savings of four states in the controller dynamics.

Conclusions

A fixed-order dynamic compensator has been designed as a longitudinal flight controller for the F-18/HARV. The controller is designed using a seventh-order linear model for a low-speed, high angle of attack hard trim point. The third-order dynamic compensator, implemented in observer canonical form, provides robustness and tracking performance at the plant output. The simulations to step command inputs illustrated that all outputs settled in approximately 4 s. The control deflections were generally less than 1.0 deg. The fixed-order compensator has been compared with a full-order observer. Both controllers have similar frequency characteristics and guarantee 60-deg phase margin and 6 dB gain margin. However, with the integral states introduced, the fixed-order compensator has only 6 states as compared with 10-state full-order design. Moreover, the full-order observer must be designed for a square plant whereas the fixed-order dynamic compensator has been designed for a nonsquare plant. For the fixed-order compensator design, the number of measurements are not constrained to be equal to the number of control inputs.

References

[1]Voulgaris, P., and Valavani, L., "High Performance Linear Quadratic and H_∞ Designs for a Supermaneuverable Aircraft," *Journal of Guidance, Control, and Dynamics,* Vol. 14, No. 1, 1991, pp. 157–165.

[2]Voulgaris, P., "High Performance Multivariable Control of the 'Supermaneuverable' F18/HARV Fighter Aircraft," M.S. Thesis, Dept. of Aeronautics and Astronautics, Massachusetts Inst. of Technology, Cambridge, MA, May 1988.

[3]Doyle, J. C., and Stein, G., "Multivariable Feedback Design: Concepts for a Classical/Modern Synthesis," *IEEE Transactions on Automatic Control,* Vol. AC-26, Feb. 1981, pp. 4–10.

[4]Doyle, J. C., Glover, K., Khargonekar, P. P., and Francis, B. A., "State Space Solutions to Standard H_2 and H_∞ Control Problems," *IEEE Transactions on Automatic Control,* Vol. AC-34, Aug. 1989.

[5]Byrns, E. V., Jr., and Calise, A. J., "Approximate Recovery of H_∞ Loop Shapes Using Fixed Order Dynamic Compensation," AIAA Guidance, Navigation, and Control Conference, New Orleans, LA, Aug. 1991 (AIAA Paper 91-2729).

[6]Calise, A. J., and Prasad, J. V. R., "An Approximate Loop Transfer Recovery Method for Designing Fixed Order Compensators," *Journal of Guidance, Control, and Dynamics,* Vol. 13, No. 2, 1990, pp. 297–302.

[7]Kramer, F. S., and Calise, A. J., "Fixed Order Dynamic Compensation for Multivariable Linear Systems," *Journal of Guidance, Control, and Dynamics,* Vol. 11, No. 1, 1988, pp. 80–85.

[8]Calise, A. J., and Byrns, E. V., Jr., "Output Loop Transfer Recovery for Fixed Order Dynamic Compensators," American Control Conference, San Diego, CA, May 1990.

[9]Mendel, J. M., "A Concise Derivation of Optimal Constant Limited State Feedback Gains," *IEEE Transactions on Automatic Control,* Vol. AC-19, Aug. 1974, pp. 447–448.

[10]Moerder, D. D., and Calise, A. J., "Convergence of a Numerical Algorithm for Calculating Optimal Output Feedback Gains," *IEEE Transactions on Automatic Control,* Vol. AC-30, Sept. 1985, pp. 900–903.